On Severe Downslope Winds

RONALD B. SMITH

Yale University, New Haven, CT

(Manuscript received 4 April 1985, in final form 24 June 1985)

ABSTRACT

Recent observations and numerical experiments indicate that during severe downslope windstorms, a large region of slow turbulent air develops in the middle and upper troposphere while strong winds plunge underneath. A mathematical model of this severe wind state is developed using Long's equation. This theory predicts the altitude of the turbulent air, the strength of the winds, and the mountain drag. In the presence of a wind reversal, the theory indicates which wind reversal altitudes will lead to windstorm conditions.

1. Introduction

Reports of severe windstorms on the lee side of major mountain ranges continue to appear, yet the aerodynamics of these events is poorly understood. The mountain wave studies of Lyra (1943) and Queney (1948) almost certainly provide the starting point for these investigations, but their results are not directly applicable because of the small amplitude assumption used in those analyses. In 1953 and 1955, R. R. Long presented a mathematically linear equation governing steady mountain waves of large amplitude, along with some solutions in bounded geometries. The utility of this approach is widely recognized and other solutions to Long's equation have been reported; e.g., the solution in a half space by Miles and Huppert (1969).

Observations of severe downslope winds have come from many sites around the world, but the most well-known is the Boulder windstorm. This is due in part to the strength of the phenomenon there and in part to the concentration of atmospheric scientists in that city. One nicely documented case is the 11 January 1972 windstorm (Lilly, 1978) in which research aircraft discovered that the entire tropospheric airflow was descending and passing over Boulder in a layer only two kilometers deep!

Recently there have been two major attempts at constructing a theory of downslope windstorms. Klemp and Lilly (1975), extending the work of Blumen (1965), using the small amplitude equations and accounting for vertical variations in wind and stability, showed that certain upstream conditions would lead to partial resonance and thus to strong mountain wave response. In their analysis, partial reflection from the tropopause often played a role in this. Their theory seems to have some predictive power although the estimation of the wave phase shift and reflection coefficient needed to determine resonance is inexact because of finite mountain height, streamline displacement, and tropopause thickness.

In a series of papers, T. L. Clark and W. R. Peltier (1977, 1979, 1980, 1984) solved the equations of motion numerically for systematically chosen sets of initial conditions. Their most important result was the identification of a separate "high drag" or "severe wind" flow configuration. For example, with uniform wind and stability upstream, and with a mountain height so great that wave breaking will occur, the flow begins to evolve in time approaching a new "severe wind" configuration, very different from the linear theory or the Miles and Huppert solutions of Long's equation. This new state is characterized by strongly accelerated low level flow, a region of weak winds and strong turbulence in the middle or upper troposphere, and weaker waves aloft. They went on to reason, in a way roughly parallel to Klemp and Lilly, that the high drag state is associated with a partial resonance. In this case, they associated the high drag state with wave reflection from the turbulent region.

The present paper describes a new attempt to construct a theory of severe downslope winds. The theory makes use of Long's equation in the strongly disturbed low-level flow. An idealized picture of the severe wind configuration, as derived from the observations of Lilly (1978) and the numerical calculations of Peltier and Clark (1979), is used to determine the appropriate upper boundary condition. Together these two features lead to a theory similar to the internal hydraulic theories of Yih (1965), Long (1970), Baines (1977) and others, but with a few essential differences.

2. The severe wind configuration

Consider the idealized description of the severe wind configuration shown in Fig. 1. The streamline or θ-surface originating at some level H_0 splits over the

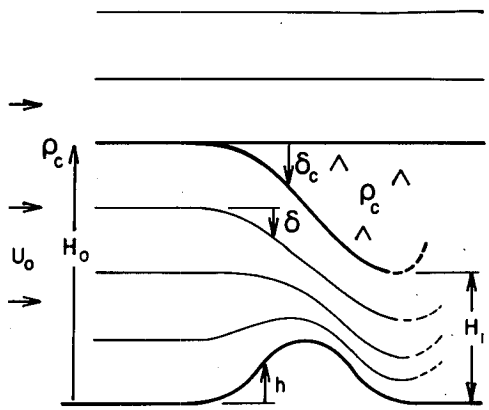

FIG. 1. Schematic of the idealized high-drag flow configuration, derived from aircraft observations and numerical simulations. A certain critical streamline divides and encompasses a region of uniform density. The disturbance aloft is small compared to that below.

mountain with the lower branch descending rapidly. Above H_0 only weak waves are present, at least in comparison with the strong perturbations below. Between the split streamlines, the air has little mean motion but considerable turbulence and is well mixed with a potential temperature equal to θ_c (or a density of ρ_c in a Boussinesq model). Below the lower ψ_c streamline, the flow is assumed to be smooth, nondissipative, hydrostatic, Boussinesq and steady. As the upstream flow is assumed to have constant speed U_0 and stability N_0, the governing equations reduce to

$$\delta_{zz} + l^2\delta = 0 \tag{2.1}$$

(Long, 1955) where $\delta(x, z) = z - z_0$ and z_0 is the upstream altitude of the streamline through the point (x, z). The parameter $l = N_0/U_0$. If the function $\delta(x, z)$ is known, the horizontal velocity can be obtained from

$$u = U_0(1 - \delta_z). \tag{2.2}$$

The lower boundary condition is

$$\delta[x, h(x)] = h(x) \tag{2.3}$$

where $h(x)$ describes the height of the terrain above the zero level. The upper boundary condition is determined as follows. If there is no (or small) disturbance above H_0, the pressure at $z = H_0$ is constant

$$p(x, H_0) = p^*. \tag{2.4}$$

If the air in the turbulent region is hydrostatic in the mean and well mixed with $\rho = \rho_c$, then the pressure along the lower branch of the split streamline is

$$p(x, H_0 + \delta_c) = p^* - \rho_c g\delta_c \tag{2.5}$$

where δ_c is the (positive upwards) vertical displacement of the lower dividing streamline. Bernoulli's equation along this streamline

$$p + \frac{1}{2}\rho u^2 + \rho_c gz = \text{constant} \tag{2.6}$$

with (2.4) and (2.5) gives

$$u(x, H_0 + \delta_c) = U_0 \tag{2.7}$$

or with (2.2)

$$\delta_z = 0 \quad \text{at} \quad z = H_0 + \delta_c. \tag{2.8}$$

Now, if we write the solution to (2.1) as

$$\delta(x, z) = A(x)\cos lz + B(x)\sin lz$$

and introduce nondimensional coefficients and parameters $\hat{h} = lh$, $\hat{H}_0 = H_0 l$, $\hat{\delta}_c = \delta_c l$, $\hat{A} = Al$, and $\hat{B} = Bl$, then conditions (2.3) and (2.8) can be written as three, canonical nonlinear equations

$$\hat{h} = \hat{A}\cos\hat{h} + \hat{B}\sin\hat{h} \tag{2.10}$$

$$0 = -\hat{A}\sin(\hat{H}_0 + \hat{\delta}_c) + \hat{B}\cos(\hat{H}_0 + \hat{\delta}_c) \tag{2.11}$$

$$\hat{\delta}_c = \hat{A}\cos(\hat{H}_0 + \hat{\delta}_c) + \hat{B}\sin(\hat{H}_0 + \hat{\delta}_c). \tag{2.12}$$

These in turn can be rearranged to give

$$\hat{h} = \hat{\delta}_c[\cos(\hat{H}_0 + \hat{\delta}_c - \hat{h})] \tag{2.13}$$

$$\hat{A} = \hat{\delta}_c\cos(\hat{H}_0 + \hat{\delta}_c) \tag{2.14}$$

$$\hat{B} = \hat{\delta}_c\sin(\hat{H}_0 + \hat{\delta}_c). \tag{2.15}$$

With $\hat{h}$ and $\hat{H}_0$ specified, (2.13) can be solved graphically or numerically by successive approximations to find $\hat{\delta}_c$ and then (2.14) and (2.15) are used to find $\hat{A}$ and $\hat{B}$. Solution curves for (2.13) are shown in Fig. 2. One tabulated solution curve (for $\hat{H}_0 = 3\pi/2$) is given in Appendix A.

Two properties of these solutions are evident from (2.13)–(2.15). First, if a set $\hat{\delta}_c$, $\hat{A}$, $\hat{B}$ is a solution with specified $\hat{h}$ and $\hat{H}_0$, then it is also a solution with $\hat{h}$ and $\hat{H}_0 + 2\pi m$ (m an integer) as $\hat{H}_0$ appears only within trigometric functions with period 2π. Second, for small $\hat{h}$ and $\hat{\delta}_c$ the solution to (2.13)–(2.15) is

$$\hat{\delta}_c = \hat{h}/\cos\hat{H}_0$$

$$\hat{A} = \hat{h}$$

$$\hat{B} = \hat{h}\tan\hat{H}_0. \tag{2.16}$$

The singularities in (2.16) at $\hat{H}_0 = \pi/2 + \pi m$ correspond to linear theory internal wave resonances with a free upper boundary, but these points are important here only because they separate different types of finite amplitude behavior.

In Fig. 2, the fourth quadrant is of particular interest as it includes all the cases where a "positive" mountain can produce transition to a shallower faster flow. Consider, for example, an $\hat{H}_0$ between $\pi/2$ and $3\pi/2$. As $\hat{h}$ increases from zero, $\hat{\delta}_c$ becomes negative. If the maximum mountain height $\hat{h}_m$ is too small, $\hat{\delta}_c$ will return to zero as $\hat{h}$ does, in a reversible manner. If $\hat{h}_m$ is just equal to the turning value for the given $\hat{H}_0$, the value of $\hat{\delta}_c$ may continue to drop as $\hat{h}$ returns to zero. In the

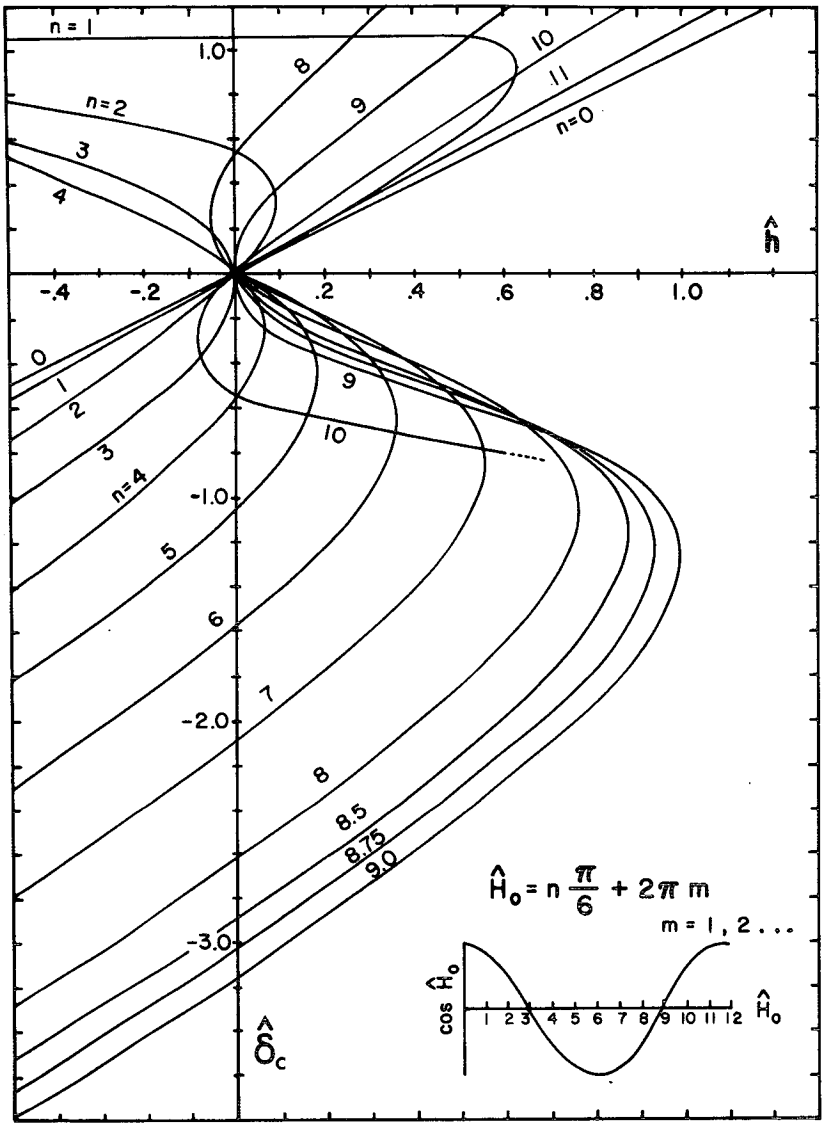

FIG. 2. Solution curves for Eq. (2.13) plotted as terrain height ($\hat{h} = hl$) against deflection of the critical streamline ($\hat{\delta}_c = \delta_c l$). Each curve is for a different upstream height ($\hat{H}_0 = H_0 l$). Curves in the fourth quadrant represent flows which can transition to faster flow over positive terrain. For clarity, not all the curves are carried through the origin.

case where the final terrain height is the same as upstream, the new stream has simple properties

$$\left.\begin{aligned} \hat{H}_1 &= \frac{\pi}{2}, \quad \hat{\delta}_{c_1} = \frac{\pi}{2} - \hat{H}_0 \\ \hat{A} &= 0, \quad \hat{B} = \hat{\delta}_{c_1} \\ \delta(x_1, z) &= \delta_{c_1} \sin lz \\ u(x_1, z) &= U_0(1 + \hat{\delta}_{c_1} \cos lz) \end{aligned}\right\}. \tag{2.17}$$

To allow for cases where the final terrain height drops below its upstream value, the transition curves in Fig. 2 have been extended into the third quadrant. Examples of both situations are shown in Figs. 3 and 4. In both cases $\hat{h}_m$ is chosen to be unity, the largest value for which transitional solutions exist for positive mountains. These plots correspond to curve $n = 9$ in Fig. 2, with $\hat{H}_0 = 3\pi/2$.

The vertical coordinate in Figs. 3 and 4 is the nondimensional $\hat{z} = lz$, but dimensional values are also given for the case $U_0 = 20$ m s^{-1} and $N_0 = 0.01$ s^{-1}. Interpreted this way, there is a qualitative similarity between these figures and the Boulder storm observations and previous numerical simulations. The initial height of the dividing streamline is reasonable. The descent of the lower dividing streamline begins over the point where the mountain begins to rise. This descent becomes more rapid over the mountain peak.

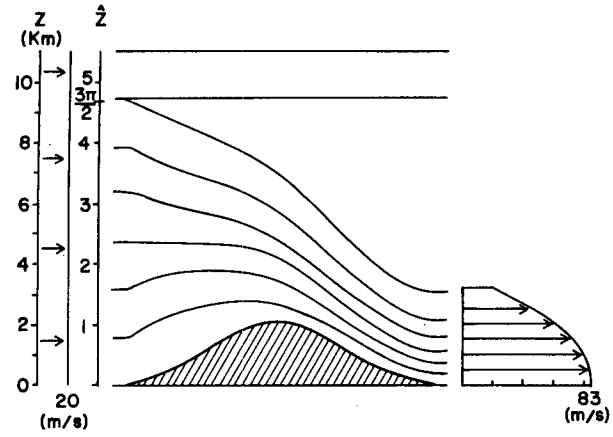

FIG. 3. Transitional flow over a mountain of maximum height $\hat{h}_m = 1$ which returns to its original height downstream. Dimensional values of altitude and wind speed are given for the case of $U_0 = 20$ m s^{-1}, $N_0 = 0.01$ s^{-1}.

The final downward displacement of the dividing streamline is a large fraction of the initial layer depth. The air speed after transition is greatest near the ground and is several times the upstream value. Unfortunately, the theory does not show what happens farther downstream as the flow rebounds, presumably in a turbulent way, to fill the troposphere. Dissipation, unsteadiness, or nonhydrostatic behavior in that region would invalidate (2.1). Such effects might even begin before the mountain is past.

Another measure of strength of the transitional flow is the pressure drag on the mountain per unit length. This can be unambiguously defined only for a case like Fig. 3 where the mountain rises out of a common plain. Then an expression for the drag can be derived from a control volume momentum budget (see Appendix B),

$$D = \frac{\rho N^2}{6}(H_0 - H_1)^3. \tag{2.18}$$

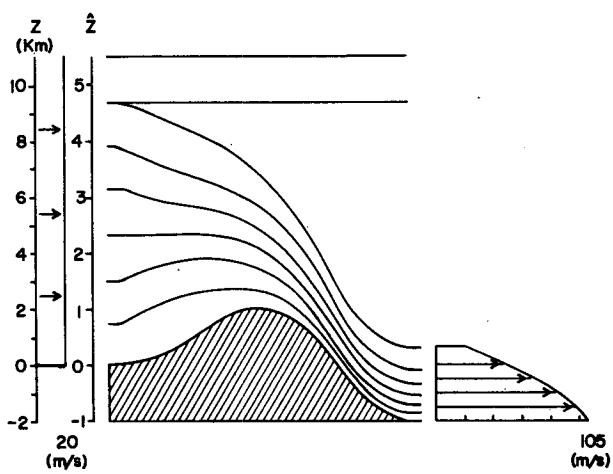

FIG. 4. As in Fig. 3 but for a mountain which drops to new lower level, allowing a further acceleration of the surface winds.

Using (2.17) and parameter settings $U_0 = 20$ m s^{-1}, $N_0 = 0.01$ s^{-1}, $h_m = 2$ km so that $\hat{H}_0 = 3\pi/2$, $\hat{H}_1 = \pi/2$, (with $\rho = 1$ kg m^3) the value

$$D = 4136 \times 10^3 \text{ kg s}^{-2}$$

is obtained corresponding to Fig. 3. This is equivalent to an average pressure difference across the mountain of 21 mb.

Consider now the conditions under which transitional flow can exist. From Fig. 2 it is clear that for each mountain height $\hat{h}_m$ only one $\hat{H}_0$ is allowed ($+2\pi m$ of course). This relationship is shown explicitly in Fig. 5. Since $\hat{h}_m$ is predetermined, the corresponding $\hat{H}_0$ must be selected by the flow. For example, if $\hat{h} = 0.9$, $\hat{H}_0$ will be about 4.5. Since nothing in the present theory indicates when mountain airflow will evolve into the severe wind state, we must speculate with Clark and Peltier (1984, hereafter CP84) that this will occur for values of $\hat{h} \geq 0.85$, the Miles and Huppert value for wave breaking. Figure 5 then predicts that $\hat{H}_0$ will lie between about 4.4 and 4.71, values just slightly less than $3\pi/2$.

Values of $\hat{H}_0$ near $3\pi/2$ were found by Clark and Peltier (1977, 1979) in their numerical experiments but they offered a different explanation. They noted that for a symmetric mountain, initial wave breaking begins near $\hat{z} = 3\pi/2$, and suggested that this would carry over to the final high drag state. The present analysis suggests instead that this height is an intrinsic property of the severe wind configuration. A method for testing this point was suggested by Lilly and Klemp, 1980. They proposed using an asymmetric mountain so that the initial wave breakdown would occur at a different level. This numerical calculation has apparently not yet been carried out.

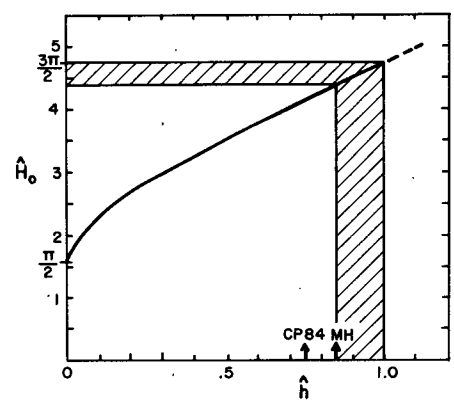

FIG. 5. Corresponding values of mountain height ($\hat{h}$) and upstream altitude of dividing streamline ($\hat{H}_0$) which allow transition. These values are taken from the maxima in Fig. 2. Arrow "MH" indicates the mountain height where breaking begins in Long's problem according to Miles and Huppert (1969). Naturally occurring high drag states would probably lie near this point or beyond (shaded region). Arrow "CP84" indicates the mountain used by Clark and Peltier (1984), with breaking near a wind reversal in the environment.

According to Fig. 5, transitional flows for mountains higher than $\hat{h}_m = 1$ are not possible. The interpretation of this is not clear but a plausible suggestion is that for higher mountains a blocked layer might form upstream returning the effective $\hat{h}_m$, now measured from the top of the blocked layer, to unity. The choice of $\hat{h}_m = 1$ as a criterion for blocking is quantitatively not very different than that arising from other types of analysis.

Another constraint in the present model is the onset of Kelvin–Helmholtz instability in the accelerating flow. The stability criterion $\mathrm{Ri} \equiv N^2/U_z^2 > \frac{1}{4}$, will first be violated along the upper streamline of the descending flow $z = H_0 + \delta_c$ as $N = N_0$ there, and $|U_z|$ is a maximum. The Ri decreases smoothly along this streamline, reaching a minimum at the downstream position (x_1). Using (2.1) and (2.2), we can write

$$\mathrm{Ri}(x, H_0 + \delta_c) = \hat{\delta}_c^{-2} \tag{2.19}$$

so that Kelvin–Helmholtz instability is possible when the streamline drops to where $|\hat{\delta}_c| > 2$ (note where this lies on Fig. 2). For cases like Fig. 3 where $h(x_1) = 0$, the Richardson number decreases to (using 2.17)

$$\mathrm{Ri}(x_1, H_1) = (\hat{H}_0 - \pi/2)^{-2}. \tag{2.20}$$

Thus for $\hat{H}_0 > 2 + \pi/2$ (i.e., $\hat{h}_m \geq 0.5$ from Fig. 5) Kelvin–Helmholtz instability is likely to begin aloft before the end of the mountain is reached.

3. Flows with a wind reversal

In the previous section we have considered only uniform incoming flow. Clark and Peltier (1984) suggested that a deeper understanding could be obtained by including a wind reversal in the environment as a way to preset the breaking level. They followed this up with a series of numerical experiments with wind reversals at different altitudes (z_c) and a mountain height chosen so that wave breaking will only occur in the slower flow near the wind reversal. The results are quite remarkable (Fig. 6). Most values of z_c give a drag near the linear theory value $D = (\pi/4)\rho N U h_m^2$, or the Long's model value, but in two narrow peaks it increases by a factor of 3 or more.

The present theory can be used to partially explain these results. With values $h_m = 300$ m, $U_0 = 8$ m s^{-1}, $N_0 = 0.02$ s^{-1} the nondimensional $\hat{h}_m = 0.75$. From Fig. 5 this requires $\hat{H}_0 = 4.15$, 10.43, etc., for transitional flow. The hypothesis $\hat{H}_0 = \hat{z}_c$ allows these values to be plotted (as bars) on Fig. 6. The magnitude of the drag, computed from (2.15), is indicated by the height of the bar. The theory gives no prediction of the range of the high drag regime so the width of the bar is arbitrarily chosen. The determination of this range would probably require a time dependent model capable of describing the upstream adjustment processes. In a numerical model, the range of $\hat{z}_c$ which allows strong re-

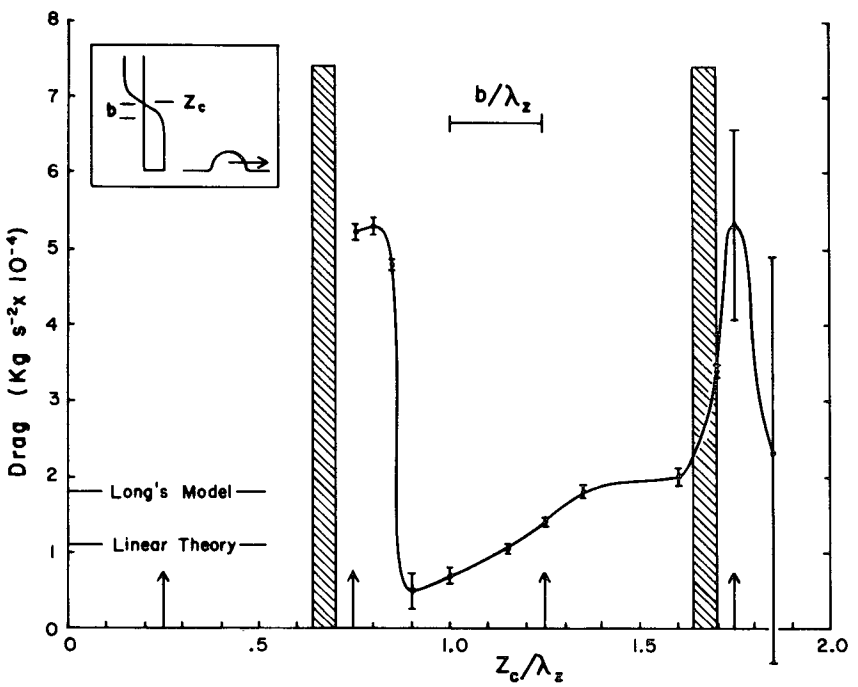

FIG. 6. Computed drag for flow with a wind reversal, from CP84, and the predictions of two theories. Columns indicate position and magnitude of hydraulic high drag flow with the hypothesis $H_0 = z_c$ and with $h = 300$ m, $U = 8$ m s^{-1}, $N = 0.025^{-1}$. Arrows indicate position of linear theory resonances associated with a free reflection at z_c. Horizontal error bar indicates uncertainty in the effective z_c due to the width of shear zone.

sponse may depend on the horizontal dimension of the domain and the nature of the lateral boundary conditions.

It appears from Fig. 6 that the theoretical predictions qualitatively agree with the numerical results of CP84. Quantitatively, the predicted drag is too high and the peak slightly offset. The offset is explained if the dividing streamline is assumed to fall within the shear zone, but slightly below the zero wind point z_c in the basic state. The lower drag in the numerical experiment might be due to onset of the turbulent jump before the mountain is past.

Clark and Peltier (1984) explain these peaks as resonances associated with wave reflection from the critical level. This would lead to linear theory singularities at $\hat{z}_c = \pi/2, 3\pi/2, 5\pi/2, 7\pi/2$, etc. (that is $z_c/\lambda_z = 0.25$, 0.75, 1.25, 1.75, etc.) if the reflection is from a "free" constant pressure boundary with a reflected phase shift of π. These values are shown as arrows in Fig. 6. A serious objection to the resonance cavity idea, then, is the prediction of a high drag peak near $z_c/\lambda_z = 1.25$ and its absence in the numerical results.

What is the relationship between the linear theory "free boundary" resonances and the finite amplitude theory? As shown in Section 2, the linear resonances do appear as special points in the finite amplitude hydraulic theory as we have used a free boundary there as well. In the hydraulic theory, however, the free boundary condition is not applied at a fixed level giving a coherent reflection, but rather along a greatly deflected streamline of the flow. The observed clustering of $\hat{H}_0$ values near $3\pi/2$ has nothing to do with the linear resonance there but in a sense is a finite amplitude extension of the $\pi/2$ singularity (see Fig. 5 for evidence of this).

4. Flows with variable wind and stability

The outstanding problem regarding severe downslope winds is the prediction of when they will occur. The present theory, while it can predict certain aspects of the severe wind structure, is primarily a consistency analysis and provides little help here. One simple argument would be to assume that the CP84 result applies more broadly; that is, whenever wave breaking is predicted from a linear or Long's Model solution, the flow will evolve instead to a severe wind configuration. If, using the language of nonlinear systems analysis, the severe wind configuration has a large enough "domain of attraction," it would not particularly matter exactly where or how the wave breaking began. This possibility would allow the Klemp and Lilly (1975) linear resonant reflection condition to play a role in the prediction of severe winds even though it probably has no application to the final severe wind configuration.

Another way in which the atmospheric structure might trigger the severe wind state is through the action of a middle level inversion. The ubiquity of this feature was discussed by Brinkman (1973) in relation to Boulder windstorm climatology. If the Froude number based on the height and strength of this inversion (Fr $= U/\sqrt{g'H}$) is less than one but not too small, then hydraulic acceleration and transition of the classical type could lead to a jump on the lee side, initiating the evolution to the severe state.

Further discussion of triggering and evolution to a severe state is probably premature. It is based on an untested assumption (that all wave breaking cases would evolve to severe conditions) and ignores the effect of atmospheric structure on the final severe wind state itself. Further numerical experiments of the type done by Clark and Peltier are needed. The role of atmospheric structure and the possibility of hysteresis need to be investigated.

5. Conclusion

The purpose of this analysis is to provide a mathematical description of the severe wind state. For uniform incoming flow, the theory can reasonably predict the height of the dividing streamline, the depth of the turbulent zone, the wind speed and pressure as functions of position, the location of Kelvin–Helmholtz instability, and the total drag. For a subcritical mountain height ($\hat{h}_m < 0.85$) and with an environmental wind reversal, the theory reasonably predicts the height of the wind reversal level which will lead to a severe wind state, and the structure and drag of that state. The theory is currently limited to uniform incoming wind and stability and therefore provides only a qualitative understanding of real atmospheric flows. Furthermore, by itself, it does not offer a way to predict the occurrence of severe downslope winds.

The success of the theory leaves us with a new view of the dynamics of severe downslope winds. The severe wind state exists by means of an interaction between strong smooth stratified flow and a deep turbulent mixed "dead" region.

Acknowledgments. The author is indebted to D. K. Lilly for suggesting more compact forms for equations (2.13)–(2.15) and (2.18). This work was supported by the National Science Foundation under Grant ATM-8303632.

APPENDIX A

A Tabulated Solution Curve

For use in constructing sample solutions, one solution curve is given below in tabular form. These solutions are for $\hat{H}_0 = 3\pi/2$, the case plotted in Figs. 3 and 4.

$\hat{h}$	$\hat{\delta}_c$	$\hat{A}$	$\hat{B}$	$\hat{\delta}_c$	$\hat{A}$	$\hat{B}$
−1.0				−4.48	−4.13	−1.46
−0.9				−4.26	−3.81	−1.88

APPENDIX A (*Continued*)

$\hat{h}$	$\hat{\delta}_c$	$\hat{A}$	$\hat{B}$	$\hat{\delta}_c$	$\hat{A}$	$\hat{B}$
−0.8				−4.14	−3.47	−2.26
−0.7				−4.02	−3.08	−2.57
−0.6				−3.90	−2.66	−2.82
−0.5				−3.78	−2.23	−3.03
−0.4				−3.65	−1.79	−3.20
−0.3				−3.53	−1.32	−3.26
−0.2				−3.40	−0.88	−3.31
−0.1				−3.27	−0.43	−3.21
0.0	0	0	0	−3.14	0	−3.14
+0.1	−0.27	0.08	0.26	−3.01	0.41	−3.04
0.2	−0.37	0.13	0.35	−2.87	0.77	−2.77
0.3	−0.44	0.19	0.40	−2.73	1.09	−2.52
0.4	−0.51	0.25	0.44	−2.59	1.36	−2.19
0.5	−0.57	0.31	0.48	−2.44	1.58	−1.85
0.6	−0.64	0.38	0.51	−2.28	1.74	−1.47
0.7	−0.71	0.46	0.54	−2.10	1.81	−1.06
0.8	−0.80	0.57	0.56	−1.91	1.80	−0.63
0.9	−0.93	0.75	0.56	−1.67	1.67	−0.17
0.95	−1.04	0.90	0.53	−1.51	1.51	+0.09
0.97	−1.11	1.00	0.49	−1.42	1.40	+0.21
0.98	−1.17	1.08	0.45	−1.35	1.32	+0.30
0.99			No Solution			

APPENDIX B

The Initial and Final Density and Pressure Fields and Mountain Drag

In the undisturbed flow the density and pressure are given by

$$\rho_0 = \rho_c + \rho_z(z - H_0)$$

$$p_0 = p^* + g\rho_c(H_0 - z) - \tfrac{1}{2} g\rho_z(z - H_0)^2$$

where p_0^* the pressure at $z = H_0$. After transition to an accelerated flow with h again equal to zero,

$$\rho_1 = \rho_c + \rho_z(z - \delta_c - H_0)$$

$$p_1 = p_1^* + g\rho_c(H_1 - z) + g\rho_z \times \left[\frac{H_1^2 - z^2}{2} - (H_1 - H_2)l^{-1}\cos lz - H_0(H_1 - z_1)\right]$$

where we have used $\cos lH_1 = 0$ and $p_1^* = p_0^* + g\rho_c(H_0 - H_1)$.

Using these, we note that the horizontal pressure force on the layer upstream and downstream of the obstacle is

$$PF_0 = p_0^* H_0 + \tfrac{1}{2} g\rho_c H_0^2 - \tfrac{1}{6} g\rho_z H_0^3$$

$$PF_1 = p_1^* H_1 + \tfrac{1}{2}\rho g_c H_1^2 + g\rho_z\left[\frac{H_1^3}{3} - (H_1 - H_0)l^{-2} - H_0\frac{H_1^2}{2}\right].$$

The momentum flux crossing the same stations:

$$\left.\begin{aligned} MF_0 &= \rho U_0^2 H_0 \\ MF_1 &= \rho U_0^2[H_1 - 2(H_1 - H_0) + (H_1 - H_0)^2 l^2 H_1/2] \end{aligned}\right\}.$$

Finally, the drag:

$$D = (PF_0 - PF_1) + (MF_0 - MF_1) - F^*$$

where $F^* = P_0^*(H_0 - H_1) + g\rho_c(H_0 - H_1)^2/2$ is the pressure force on the layer from the mixed region. This reduces to

$$D = \frac{\rho N^2}{6}(H_0 - H_1)^3.$$

Note that this formula also applies if $h(x)$ returns to zero without causing flow transition, but in this case $H_1 = H_0$ and $D = 0$.

REFERENCES

Baines, P. G., 1977: Upstream influence and Long's model in stratified flows. *J. Fluid Mech.*, **82**, 147–159.

Blumen, W., 1965: A random model of momentum flux by mountain waves. *Geofys. Publ.*, **26**, 1–33.

Brinkman, W. A. R., 1973: A climatological study of strong downslope winds in the Boulder area, NCAR Cooperative thesis No. 27, University of Colorado, 229 pp.

Clark, T. L., and W. R. Peltier, 1977: On the evolution and stability of finite amplitude mountain waves. *J. Atmos. Sci.*, **34**, 1715–1730.

——, and ——, 1984: Critical level reflection and the resonate growth on nonlinear mountain waves. *J. Atmos. Sci.*, **41**, 3122–3134.

Klemp, J. B., and D. K. Lilly, 1975: The dynamics of wave-induced downslope winds. *J. Atmos. Sci.*, **32**, 320–339.

Lilly, D. K., 1978: A severe downslope windstorm and aircraft turbulence event induced by a mountain wave. *J. Atmos. Sci.*, **35**, 59–77.

——, and J. B. Klemp, 1980: Comments on "The evolution and stability of finite amplitude mountain waves. Part II: Surface wave drag and severe downslope windstorms." *J. Atmos. Sci.*, **37**, 2119–2121.

Long, R. R., 1953: Some aspects of stratified fluids, I. A theoretical investigation. *Tellus*, **5**, 42–58.

——, 1955: Some aspects of the flow of stratified fluids. III. Continuous density gradients. *Tellus*, **1**, 341–357.

——, 1970: Blocking effects in flow over obstacles. *Tellus*, **22**, 471–479.

Lyra, G., 1943: Theorie der stationaren Leewellenstromung in freier Atmosphare. *A. angew. Math. Mech.*, **23**, 1–28.

Miles, J. W., and H. E. Huppert, 1969: Less waves in a stratified flow. Part IV: Perturbation approximations. *J. Fluid Mech.*, **35**, 497–525.

Peltier, W. R., and T. L. Clark, 1979: The evolution and stability of finite-amplitude mountain waves. Part II: Surface wave drag and severe downslope windstorms. *J. Atmos. Sci.*, **36**, 1498–1529.

——, and ——, 1980: Reply to comments of D. K. Lilly and J. B. Klemp on "The evolution and stability of finite amplitude mountain waves. Part II: Surface wave drag and severe downslope windstorms." *J. Atmos. Sci.*, **37**, 2122–2125.

Queney, Paul, 1948: The problem of air flow over mountains: a summary of theoretical studies. *Bull. Amer. Meteor. Soc.*, **29**, 16–26.

Yih, C.-S., 1965: *Dynamics of Nonhomogeneous Fluids*, Macmillan, 306 pp.